# Fully porous 3D printed titanium femoral stem to reduce stress-shielding following total hip arthroplasty

*Sajad Arabnejad, Burnett Johnston, Michael Tanzer, Damiano Pasini**

Arabnejad, Sajad, Mechanical engineering department, McGill University, Montreal, Quebec, H3A0C3, Canada

Johnston, Burnett, Mechanical engineering department, McGill University, Montreal, Quebec, H3A0C3, Canada

Tanzer, Michael, Jo Miller Orthopaedic Research Laboratory, Division of Orthopaedics, Department of Surgery, McGill University, Montreal, Quebec, H3G1A4, Canada

*Corresponding Author: Pasini, Damiano, Mechanical engineering department, McGill University, Montreal, Quebec, H3A0C3, Canada. Phone: 514-398-6295, Fax: 514-398-7365, Email: Damiano.pasini@mcgill.ca

Author Contributions:

Sajad Arabnejad had substantial contributions to research design, finite element simulation, optimization of the hip implant, interpretation of data, and drafting the paper.

Burnett Johnston had substantial contributions to research design, design of experiment, the acquisition and interpretation of experimental data, and drafting the paper.

Michael Tanzer had substantial contributions to research design, clinical evaluation, drafting the paper and revising it critically.

Damiano Pasini had substantial contributions to problem formulation and research design, computational mechanics and implant optimization, supervision, drafting and revising the paper besides approval of the submitted and final versions.

All authors have read and approved the final submitted manuscript.

**Abstract**

Current hip replacement femoral implants are made of fully solid materials which all have stiffness considerably higher than that of bone. This mechanical mismatch can cause significant bone resorption secondary to stress shielding, which can lead to serious complications such as periprosthetic fracture during or after revision surgery. In this work, a high strength fully porous material with tunable mechanical properties is introduced for use in hip replacement design. The implant macro geometry is based off of a short stem taper-wedge implant compatible with minimally invasive hip replacement surgery. The implant microarchitecture is fine-tuned to locally mimic bone tissue properties which results in minimum bone resorption secondary to stress shielding. We present a systematic approach for the design of a 3D printed fully porous hip implant that encompasses the whole activity spectrum of implant development, from concept generation, multiscale mechanics of porous materials, material architecture tailoring, to additive manufacturing and performance assessment via in-vitro experiments in composite femurs. We show that the fully porous implant with an optimized material microstructure can reduce the amount of bone loss secondary to stress shielding by 75% compared to a fully solid implant. This result also agrees with those of the in-vitro quasi-physiological experimental model and the corresponding finite element model for both the optimized fully porous and fully solid implant. These studies demonstrate the merit and the potential of tuning material architecture to achieve a substantial reduction of bone resorption secondary to stress shielding.

Keywords: porous biomaterial, total hip arthroplasty, stress shielding, digital image correlation, additive manufacturing

## Introduction

Total hip arthroplasty (THA) is commonly used to relieve pain, restore function, and improve the quality of life for patients with compromised hip joints when conservative treatments have failed. Despite the success of THA, some of the main complications of THA, such as aseptic loosening, stress shielding, and periprosthetic fracture, remain a concern. Bone resorption secondary to stress shielding can be significant and arises from the mismatch of the mechanical properties between the implant and the surrounding native femoral bone [1; 2]. Materials currently used in hip implants, such as titanium-based alloys, cobalt chromium alloys, and 316L stainless steel, all have stiffness considerably higher than that of bone. Once a metal implant is implanted into the femur, most of the physiological loading is transferred to the implant, away from the comparatively more compliant surrounding bone. The altered load transfer in the implanted femur leads to the bone being under-loaded compared to its natural state. As a result bone, a living tissue that is sensitive to mechanotransduction, resorbs and loses mass by an adaptive process known as bone remodeling [3]. This phenomenon is termed bone loss secondary to stress shielding [1; 4]. The reduction in bone stock can lead to serious complications, including peri-prosthetic fracture, while the mismatch in modulus between the implant and the bone can result in thigh pain [5-7]. Stress shielding also reduces the quality of the remaining bone stock leading to a significantly increased risk of fracture and aseptic loosening with revision surgery, should one be required. This is particularly concerning for the future, as the number of revision THAs is projected to rise, with younger patients now undergoing THA and life expectancy also increasing.

Several attempts have been made to modify femoral stems with the goal of reducing stress shielding and its adverse complications. Approaches to reduce stress shielding are mainly based

on reducing the femoral stem stiffness. Methods to achieve this aim include: modification of the geometric profile of the implant, modification of its material properties, or a combination of both material and geometrical modifications. Geometric modifications include geometric variation of the stem cross section [8-10], stem length reduction [5; 11; 12], taper and/or curvature along the femoral stem [8; 13], attachment of a collar or anchor at the proximal portion of the stem [14; 15], and adoption of a hollow stem profile and internal grooves [1; 13; 16]. Modifications of material properties include stem concepts with graded cellular materials from both cobalt chrome alloys as well as titanium alloys [17-22]. Some existing works on porous materials focus on their use as surface coating on the implant to allow bone ingrowth to achieve biologic fixation [23; 24]. Other works attempt to use porous materials for bone replacement, but they are mainly limited to computational modeling [25; 26], manufacturing and testing of small samples [19; 27; 28], morphological characterization [29-31], and proof-of-concept implants with uniform porosity [19; 20; 32]. So far, no work has successfully tackled the challenge of using a fully porous material for femoral stems. Furthermore, there is no work that has experimentally proved the merit of tuned porous architecture to reduce stress-shielding in an implanted femur. Herein we present a systematic approach for the design of a fully porous hip implant that encompasses the whole activity spectrum of implant development, from concept generation, multiscale mechanics of porous materials, material architecture tailoring, to 3D implant manufacturing and performance assessment via in-vitro experiments

## Material and Methods:

### Methodology of the Implant Design

Figure 1 summarizes the methodology that led to the development of the first fully porous femoral stem with tunable properties that minimize bone resorption as a result of stress shielding. A multiscale computational scheme dealing with the scale-dependent material architecture is integrated within a material tailoring scheme (Figure 1B) to locally tune the stiffness distribution

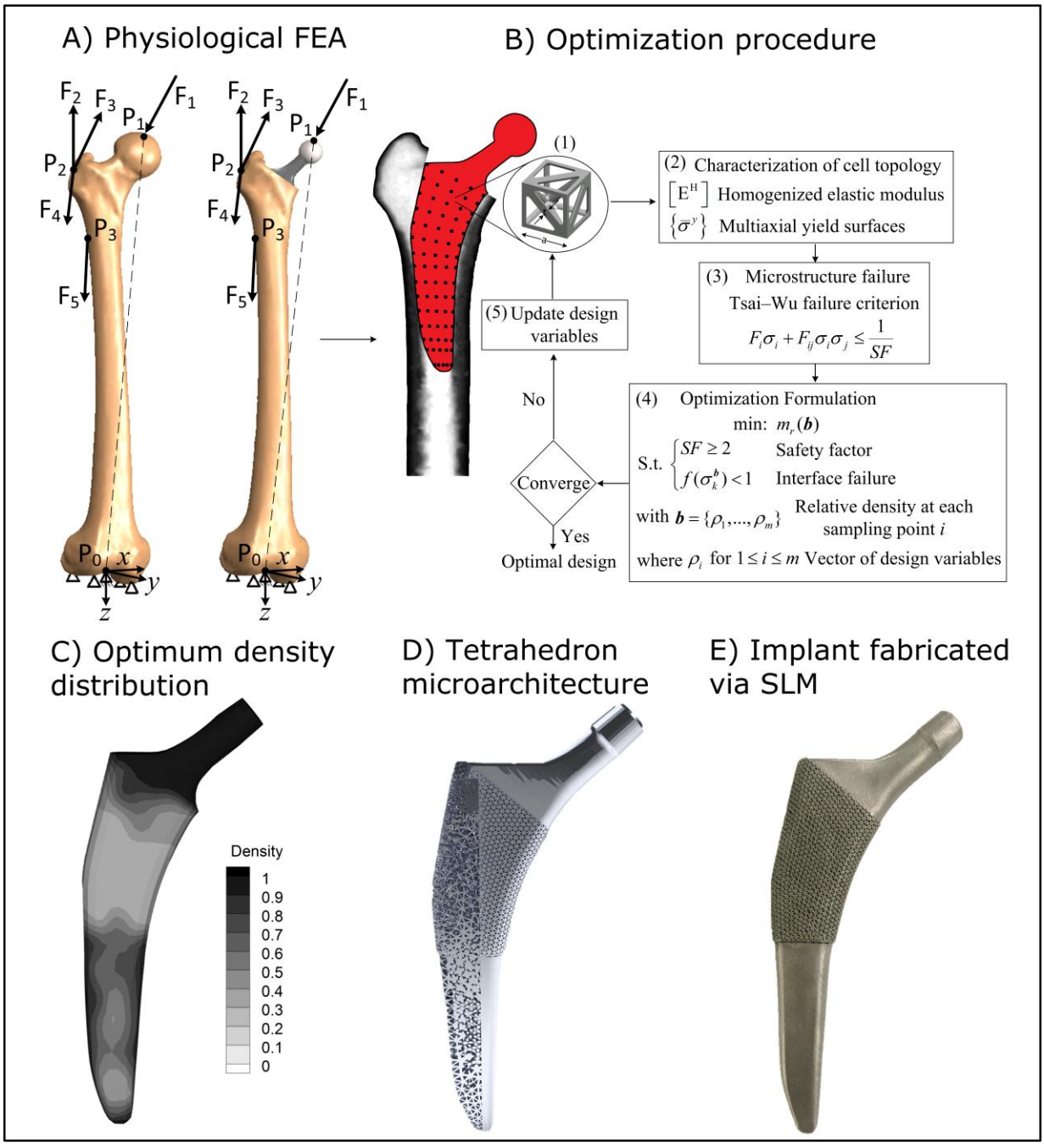


**Figure 1**: A) Physiological FEA of the implanted femur. Forces F1-5, acting forces points P0-3, and boundary conditions applied to the intact and implanted femur are during the gait cycle and are taken from [33; 34] .B) Computational scheme for multiscale mechanics and material property optimization of a minimally invasive 3D hip implant with minimum bone resorption. C) Optimum relative density distribution of the fully porous implant. D) Generation of lattice microarchitecture from optimal relative density distribution using a high strength tetrahedron topology. E) Implant manufacturing via Selective Laser Melting.

1

of the implant to those of the bone. Once an optimum relative density distribution solution is obtained (Figure 1C), the result is mapped into an architected lattice ready for manufacturing (Figure 1D). Selective Laser Melting (SLM) is used to build the implant (Figure 1E), and micro-CT analysis of the manufactured implant is performed to assess the fidelity of the implant microstructure as well as to detect any entrapment of semi or non-melted powder within the pores (Figure 2). Finally, Digital Image Correlation (DIC) test is used to assess bone resorption performance relative to a commercially available fully solid implant of identical geometry, here used as a benchmark; a complementary Finite Element (FE) model of the experiment is also created to provide volumetric context of bone loss to the experimental results (Figure 3). The multiscale design and material tailoring scheme for the design of a tuned fully porous hip implant is described in the following section.

**Multiscale design, material architecture tailoring, and physiological FEA of bone remodelling**

The procedure used to develop the porous hip implant starts from the generation of a finite element model of the femoral bone which is created by processing CT-scan data of a 38 year old patient bone. To achieve this goal, we use radiographic density of CT images, quantified as Hounsfield Unit (HU), to represent the local material properties of the human femur. The apparent density ρ for each finite element of the femur model is then determined from the Hounsfield value (HU) measured from CT data ranging from 0 HU to 1567 HU. The maximum value of HU corresponds to the densest region of the cortical bone with apparent density of 2000 kg/ $m^3$. From the apparent density distribution, the effective elastic moduli of bone are obtained through the relation [35-37]:

$$\begin{cases} E = 1904\rho^{1.64} & \rho < 0.95 \\ E = 2065\rho^{3.09} & 0.95 < \rho \end{cases}, \quad \nu = 0.3 \tag{1}$$

where E is the elastic modulus of the bone, and $\nu$ is the Poisson's ratio. Bone is treated here as isotropic material, as this simplification does not lead to a noticeable difference from those results obtained by considering orthotropic properties [36; 37]. More details on how to assign material properties to bone for finite element simulations are described in in the Supporting Information (S1).

The macro geometry of the hip implant has a tapered-wedge shape. The design domain of the prosthesis is assumed to possess a 3D lattice microarchitecture, obtained through an aperiodic tessellation of a tetrahedron based unit cell, which has been shown appropriate for both load bearing orthopaedic applications and bone ingrowth [38]. Mechanical properties, in particular the homogenized stiffness tensor $[E^H]$ and the multiaxial yield surface $\{\sigma^y\}$, are calculated via Asymptotic Homogenization (AH) theory [26; 39; 40]. We have shown that AH theory can capture stress distribution within the microstructure with a considerably higher accuracy compared to other homogenization approaches [26; 41]. The effective elastic properties and yield strength as determined by AH are detailed in the Supporting Information (S2).

To obtain the optimum relative density distribution throughout the implant to minimize bone resorption secondary to stress shielding, we discretize the 3D implant domain with 75 sampling points on the medial-lateral plane of the implant, as shown in Figure 1B and S3. The relative density at each sampling point forms the vector *b* of the design variables. To obtain the relative density distribution throughout the implant, we considered four sampling points as a 4-node bilinear quadrilateral element. The relative density of each element of the implant FE model is then obtained from the linear interpolation between the relative densities of the nodes of the 4-node bilinear element. Details on how to assign relative density distribution throughout the implant are given in Supporting Information S3.

The interior microarchitecture of the implant (Figure 1D) is obtained for a femur loaded under the physiological loading and boundary conditions[33; 34], as shown in Table 1 reporting force location and their values.

**Table 1**: Forces, acting forces points, and boundary conditions applied to the intact and implanted femur during the gait cycle (taken from [33; 34]).

| Force (N) | | | | Location (m) | | | |
|---|---|---|---|---|---|---|---|
| Load cases | X | Y | Z | Points | X | Y | Z |
| $F_1$ | -486 | -295.2 | 2062.8 | $P_0$ | 0 | 0 | 0 |
| $F_2$ | 64.8 | 104.4 | -118.8 | $P_1$ | 0.035 | 0.009 | -0.449 |
| $F_3$ | 522 | 38.7 | -778.5 | $P_2$ | -0.039 | -0.018 | -0.41 |
| $F_4$ | -4.5 | -6.3 | 171 | $P_3$ | -0.022 | -0.01 | -0.375 |
| $F_5$ | -8.1 | -166.5 | 836.1 | | | | |

Material architecture tailoring is achieved by minimizing bone resorption, $m_r(\mathrm{b})$, subjected to a set of inequality constraints, including the fatigue safety factor, $SF \geq 2$, and the interface failure, $f(\sigma_k^b) < 1$. We use the Tsai-Wu failure criterion for the failure analysis of the tetrahedron lattice under multiaxial and fatigue conditions. To design against fatigue failure, we assume the lattice microstructure to be free of defects, such as scratches, notches and nicks. As a result, the constant life diagram can be constructed to verify and design the lattice against fatigue failure [42]. Detailed formulations for multiscale and fatigue design of porous microstructure are provided in the Supporting Information S4. The amount of bone loss around the stem is determined by assessing the amount of bone that is under loaded post implantation relative to the intact femur. Bone can be considered locally under loaded when its local strain energy ($U$) per unit of bone mass ($\rho$) ($S = \frac{U}{\rho}$), is beneath the local reference value $S_{ref}$, which is the value of $S$ when no prosthesis is present. Bone resorption starts when the local value of S is beneath the value of

$(1-s)S_{ref}$ [43; 44]. $s$ is the threshold level or dead zone. In this study, the value of dead zone is set to be 0.75 [44]. The interface failure $f(\sigma_k^b)$ is expressed by $f(\sigma_k^b)=\frac{\tau}{S_s}<1$, where $\tau$ is the local shear stress at the bone-implant interface, and $S_s$ is the bone shear strength. The interface failure $f(\sigma_k^b)$ is constrained to be lower than one to ensure the bone-implant interface failure will not occur. Detailed formulation for bone loss measurement and interface failure are presented in the Supporting Information S5. Through this process of material property tailoring, an implant with tuned high strength porous architecture that realizes minimum bone resorption is obtained. The implant is then manufactured with SLM technique, as described in the following section.

**Manufacturing**

The internal micro-architecture of the implant is generated from the relative density distribution determined from the optimization process previously described. The relative density of each tetrahedron lattice is obtained by calculating the average relative density over the lattice using a Gauss quadrature integration technique with one Gauss point. SLM constraints and bone ingrowth requirements, including minimum manufacturable strut thickness, porosity, and pore size, are also considered during the development of the micro architecture. In particular, the proximal portion of the hip replacement stem is constrained for optimum pore size and porosity to allow for early and extensive bone ingrowth [38]. Pore size of 500 μm and porosity of 70% are designed on the surface of the proximal bone apposing section of the hip implant. The minimum strut thickness is constrained to 200 microns throughout the implant to ensure manufacturability. The architected fully porous implant is manufactured with Selective Laser Melting (SLM) by Renishaw AM250 (Renishaw Limited, Mississauga, ON) with a power of 200 W and energy density of 60 J/mm$^3$ (Figure 1E). The laser spot diameter is 70 μm. The powder size is between

15-50 μm, and the powder layer of 30 μm is used. The part is processed at 720 degrees Celsius under argon for 2 hours, and is removed from the build plate post treatment using EDM wire cutting.

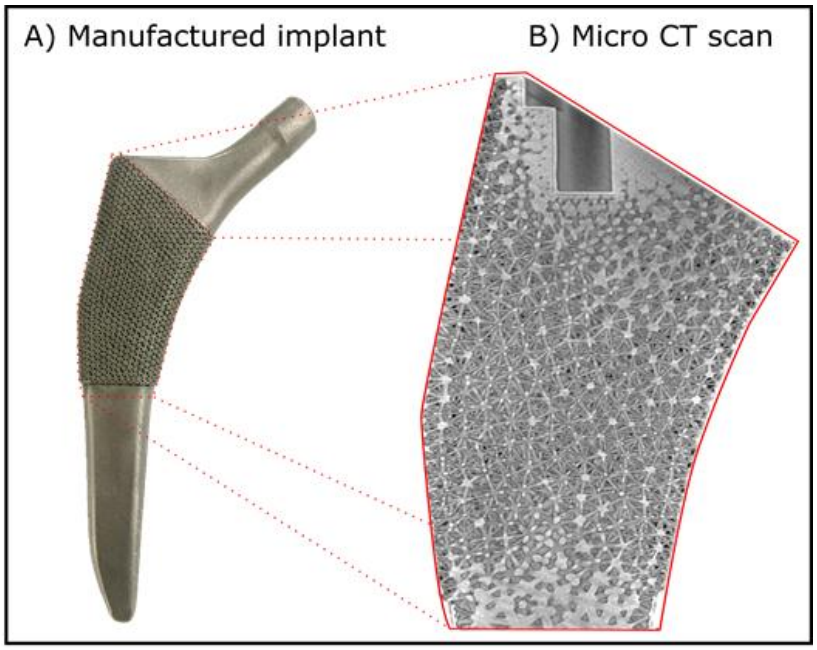


**Figure 2**: A) Implant manufacturing via Selective Laser Melting. B) Micro CT assessment of the implant lattice in the proximal region. The hole at the top left of the implant is an M6 thread which was necessary to interface with the Depuy Synthes inserter instrumentation. The inserter is identical to that of the commercial fully solid implant, and it allows to precisely control both varus-valgus as well as anteversion-retroversion positioning of the implant using the identical instrumentation that is used intraoperatively.

To assess the quality of the manufactured internal architecture, the implant is scanned using a Nikon Xt H225 ST (Nikon Canada, Mississauga, ON) (high-resolution micro-CT) (Figure 2B). Detailed inspection of CT-scan images confirms mechanical integrity of each cell strut with complete formation of all the struts with neither break nor discontinuity among the elements and absence of loose powder particles within the cell pores. To assess bone resorption performance for the manufactured implant, a benchtop biomechanical test and a complementary FE model of

the experiment are conducted to provide volumetric context of stress and strain variation in composite femora subjected to quasi-physiologic loading conditions.

**Experimental evaluation: DIC evaluation with complementary FEA**

To demonstrate the methodological approach followed in this work, a set of complementary in-vitro DIC test and computational investigations are conducted on a simplified model. The simplified model utilizes artificial composite femurs (Sawbones®, Vashon, WA) under quasi physiological loading conditions in order to minimize the variability between samples. This allows a clearly controlled experimental set up that demonstrates the experimentally measured performance of a graded fully porous implant compared to an identical clinically available fully

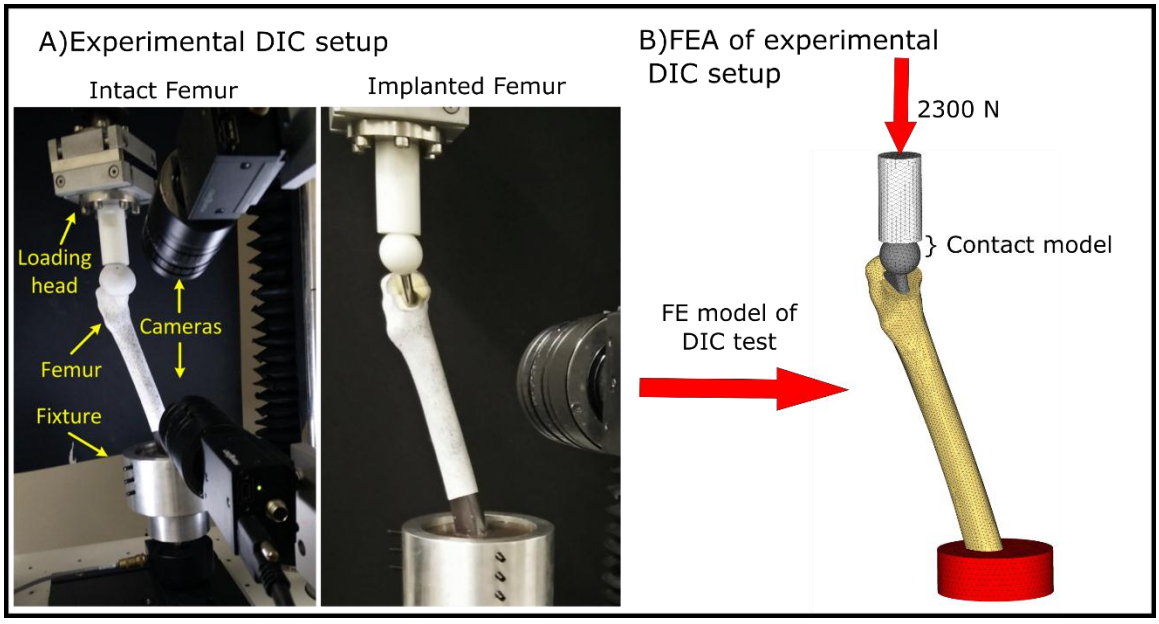


**Figure 3**: A) In-vitro assessment of stress shielding using Digital Image Correlation (DIC) and B) FE model of DIC test.

solid titanium alloy implant of equal geometry (Trilock BPS, DePuy, Warsaw, IN), our benchmark. A total of six femurs are used, with three femurs randomly allocated to each treatment to receive either the fully porous or the solid control stem. The fourth generation femurs from Sawbones® are selected for their claimed ability to reproduce a biomechanical

behavior similar to that of fresh cadaver specimens as well as low inter-specimen variability [45]. Sawbones® femurs are made of a solid material representing the cortical bone, and a foam representing the trabecular bone. Although Sawbones® femurs provide a basic tissue differentiation between the cortical and trabecular bone, we emphasize their material properties are still isotropic (E=16.7 GPa for the solid material, and E=0.155 GPa for the foam); the foam, in particular, has uniform relative density, that cannot represent the actual femoral anisotropy of native trabecular bone.

The first study considers a quasi-physiological loading pattern that can be precisely reproduced in-vitro. The goal is to compare changes in surface strain relative to an intact composite femur as a bench top experimental estimate of the expected in-vivo stress shielding. The experiment set up consists of a digital image calibration (DIC) system calibrated to measure the surface strain of both intact and implanted femurs during loading. The change of strain, measured on the medial aspect of the femur, is used as an experimental proxy for stress shielding. For the experimental preparation, all femoral condyles are resected at a distance of 22 cm measured from the tip of the greater trochanter. Using a customized fixture, the femurs are angled at 12 degrees flexion, and 12 degrees adduction and potted into epoxy (detailed description provided in the Supporting Information S6). The femoral head is loaded up to 2300N through a fixture that is free to translate within the transverse plane such that there is no un-physiological moment applied. A stereo mounted camera set up is used to acquire synchronized images of the medial calcar and medial aspect of the femur covering Gruen zones 4 through 7 [46]. The surface of the composite femora are speckle painted to achieve a distribution of speckles ranging from 500-1000 microns (Figure 3A), as described in detail in the Supporting Information S7. Images are taken at a frequency of 6Hz starting from an unloaded state, up to the maximum load at 2300N using 5 MP

CCD cameras (Point Grey Research Inc. Richmond BC) with Fujinon 25 mm c-mount lenses (Fujifilm, Valhalla, NY). From the recorded image, digital calibration is performed using Vic-3D (Correlated Solutions, Irmo, SC). The stereoscopic camera system is attached directly to an electromechanical testing frame (Bose 3510 electroforce - Bose, Eden Prairie, MN) using a custom fixture to ensure consistent camera position. The femurs are then randomly allocated to receive either the fully porous or the control stem (Supporting Information S8). An Anterior-Posterior (AP) and Medial-Lateral (ML) radiograph are taken to ensure consistent implant position, as well as correct neck offset and length (Figure S6, Supporting Information S9). The DIC data for each individual femur is exported and registered to an atlas femur using an iterative process involving closest point minimization (Figure S7-8, Supporting Information S10). This ensures that each local strain measurement is reliably and anatomically located across all femurs. To be consistent with strain energy measurements used in bone loss measurement during the design process, we considered as a metric for bone resorption, the ratio of post implantation surface strain to the pre implantation surface strain squared. Using the principle compressive strain, we can roughly estimate the strain energy of each element as follows:

$$S_{elm} = \frac{1}{2}\varepsilon_{pc}^2 E V_{elm} \tag{1}$$

where $S_{elm}$ is the strain energy of an element, $\varepsilon_{pc}$ is the principle compressive strain, $E$ is the Young's modulus of the element material, and $V_{elm}$ is the element volume. If we consider $S_{ref}$ as the local strain energy before implantation, the ratio of the strain energy of element material on the surface of the composite femur after and before implantation is:

$$\frac{S_{elem}}{S_{ref}} = \left( \frac{\varepsilon_{pc}}{\varepsilon_{pc(ref)}} \right)^2 \tag{2}$$

Equation 2 shows that the strain energy before and after implantation can be related to the ratio of the post implantation surface strain and the pre implantation surface strain squared. Therefore, in this work Equation 2 was adopted as metric for bone loss measurement on the surface of the composite femur. If the reduction of strain after implantation is greater than 50% relative to the intact femur, the bone surface region is deemed to be prone to bone resorption (Supporting Information S11). This value is chosen to coincide with the physiological FEA model value for the dead zone threshold (Supporting Information S5) used to design the architected stem (Figure 1B). The percentage of surface susceptible to bone resorption is compared between the fully porous and solid control stem for Gruen Zones 5 through 7 using a two tailed student t-test with $P<0.05$, which is considered statistically significant.

One limitation of the experimental technique described above is that only surface strain can be recorded. Bone resorption secondary to stress shielding, however, is a volumetric phenomenon. To address this issue, we conduct FE simulations replicating the experimental conditions of the implanted femur (Figure 3B) with the goal of obtaining volumetric measures of bone resorption that would supplement the surface strain measure obtained experimentally. For this purpose, a 3D model of the composite femur is created from an accurate reconstruction of CT-scan data, and FE simulations with loading and boundary conditions equivalent to those used in the experiments, are conducted in pre and post implantation conditions. The isotropic properties of the Sawbones® femur (Young's modulus: 16.7 GPa for cortical bone and 0.155 GPa for trabecular bone) are used for the computational model. The strain energy of the bone before and after implantation is measured to calculate bone loss via the criterion used during the material tailoring process. The percentage of bone loss on the bone surface is also measured and compared with the DIC results to bolster the experimental measures of bone loss in the fully

porous titanium alloy stem and the fully solid titanium alloy control stem. The results are segregated into radiological Gruen zones that are commonly used to clinically assess the performance of THA [47; 48].

## Results

### Material tailoring and physiological FEA

The material architecture tailoring described in the methodology section resulted in the optimum density distribution shown in Figure 1C. The amount of bone resorption for the optimized implant is presented in Figure 4 and compared with the amount of bone resorption of a fully solid implant. The physiological FEA model (Figure 4) shows a total of 34% of bone resorption secondary to stress shielding for the fully solid implant, and 8% percent in the optimized fully porous implant. This indicates a greater than 75% reduction in bone loss secondary to stress shielding. The fully porous implant can realize 8% volumetric bone loss in Gruen zone 7, whereas the fully solid implant 27% in zone 7, followed by 5% and 2% bone loss in Gruen zones 6 and 2 respectively. This shows that the amount of bone resorption for the fully porous implant is mainly limited to the proximal region in Gruen zone 7, whereas for the fully solid implant the amount of bone resorption extends to the distal region zone 6.

### Manufacturing

Figure 1D shows the mapping of the optimum material distribution into a tessellated tetrahedron microarchitecture. The reduced bone apposing pore size can clearly be seen, targeting an average of 500 microns for optimum bone ingrowth. CT scanning inspection shows no gross malformations of struts or entrapped un-melted powder. Figure 2B shows the CT visualization of the internal microarchitecture of the manufactured implant.

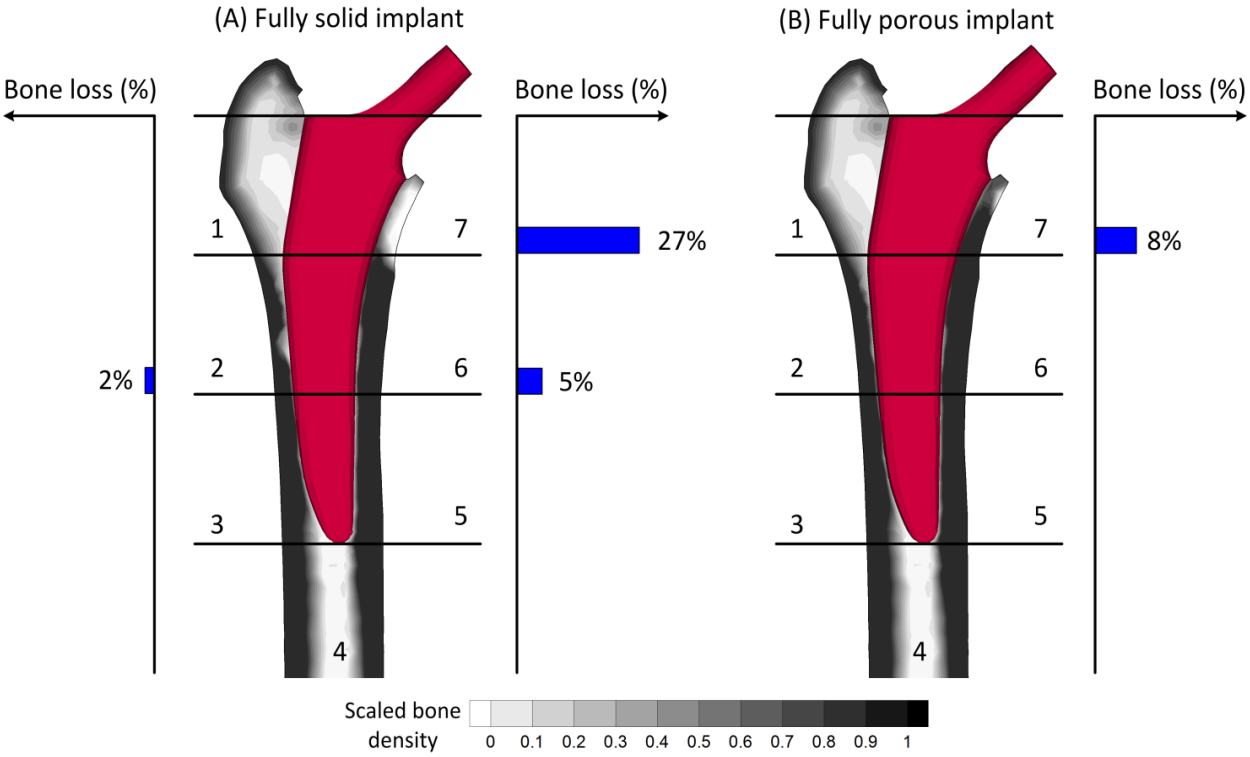


**Figure 4**: Regions prone to bone resorption in Gruen zones 1 to 7 for (A) fully solid implant and for (B) fully porous implant with tailored relative density distribution. Values presented here are volume bone loss measured from the metric described in the Supporting Information S5. All zones with no reported bone resorption are 0%.

**Experimental evaluation: DIC with complementary FEA**

Figure 5 shows the results of the quasi-physiological DIC experimental model and the corresponding FEA model for both the optimized fully porous and fully solid implant. The DIC experiment shows the greatest change in strain in the proximal medial calcar in Gruen zone 7, with bone loss of 70±24% for the fully solid implant and 71±14% for the fully porous implant ($P>0.05$). Gruen Zone 6 shows a statistically significant reduction in strain shielding for the fully porous implant as compared to the fully dense implant (25±5% vs. 7±7% $P<0.05$). Gruen zone 5 reports the least amount of strain shielding for both implants, 7±10% and 2±3% respectively for the fully solid and fully porous implants ($P>0.05$). The medial diaphysis distal

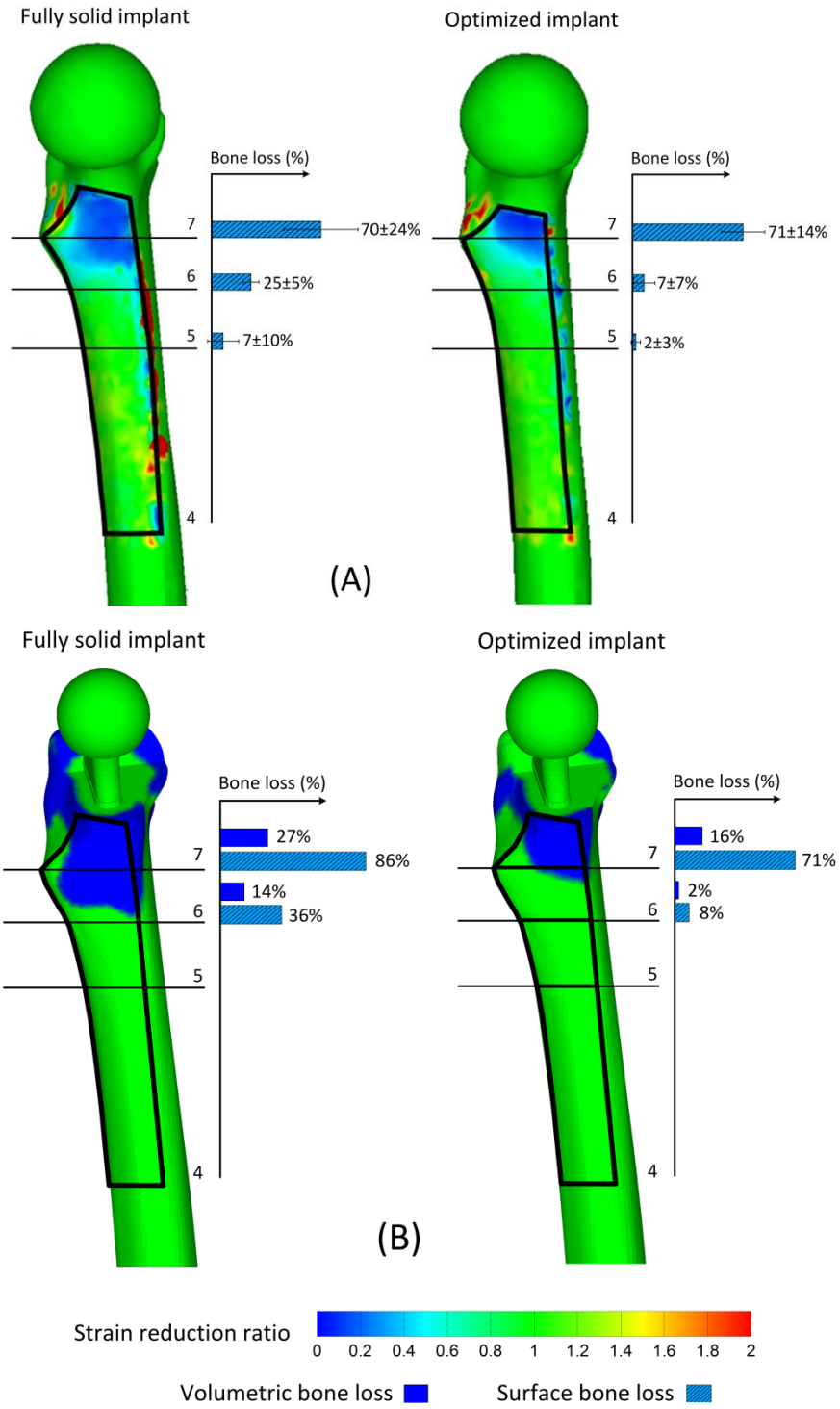


**Figure 5**: (A) Surface bone loss measurement obtained from DIC experiment. (B) surface and volume bone loss measurement from the FE model reproducing the condition of the experiment set-up. Surface bone loss is considered when the ratio of post implantation surface strain squared to the pre implantation surface strain squared decreases more than 75%. Volume bone loss is measured when the ratio of post implantation strain energy to the pre implantation strain energy decreases more than 75%.

1

to the implant shows no variation in strain from the intact femur for both the optimum and fully solid prostheses. This indicates that the neck offset is appropriately established after implantation, thereby eliminating any systematic experimental bias of the stress shielding results. The corresponding FEA model provides both surface strain reduction as well as the volumetric change of strain for both implants. Gruen zone 7 shows the largest amount of stress shielding with a 27% and 16% volumetric reduction of bone for the fully solid and optimum porous implant respectively. This shows 40% reduction of volume bone loss for the fully porous implant. In Gruen zone 6, the amount of volume bone loss for the fully solid implant is 14%; for the fully porous implant this value is equal to 2%, 78% lower than that for the baseline implant. Gruen Zone 5 shows no variation between the implanted and intact femur for both implants. At Gruen zone 7, the amount of surface bone loss for fully solid and fully porous implant is 86% and 71%, respectively. The extent of bone resorption at Gruen zone 6 for the fully dense implant is significantly higher compared to the fully porous implant. The amount of surface bone resorption for the fully porous implant is 8%, whereas for the fully solid implant this value is 36%. This shows 77% reduction of surface bone loss for the fully porous implant at Gruen zone 6 compared to fully solid implant. At Gruen zone 5, no surface bone resorption is observed for both fully porous and fully solid implant.

**Discussion**

The results from both the physiological finite element model and the DIC experiment of the current study show a reduction in stress shielding of the porous implant as compared to a fully solid stem of identical geometry. Furthermore, CT analysis shows that the optimum relative density distribution could be mapped into an aperiodic lattice domain with no entrapped un-

melted powder. This indicates that the hip implant is the first to be fully porous throughout, in contrast to existing stems with a porous coating on a solid part.

Previous designs relying on the modification of the material properties of femoral stems aimed at preserving bone stock have been used, with varying degrees of success. Isoelastic composite stems, introduced in the 1970s by Robert Mathys, were designed with a stainless steel core to improve the mechanical strength, and a polyacetal resin layer with elastic modulus similar to that of bone to avoid stress-shielding [49]. The results of 15 years follow-up revealed this prosthesis to perform extremely poorly[50]. Another composite implant is the EPOCH hip stem, which has a forged cobalt-chromium-molybdenum core section with an outer layer of pure titanium fiber metal mesh applied over a polyaryletherketone (PAEK) middle section[51]. While the data of 5 years follow up suggest that this fully porous-coated implant design provides fixation and better maintained periprosthetic cortical thickness and density than conventional implants [52], a recent study has demonstrated a 10-20% loss in peri-prosthetic bone at 7 years. This is very similar to that seen with a conventional stem [52; 53]. The authors concluded that that the merit of the Epoch stem in preserving bone mineral is only transient in nature. This can be likely attributed to the homogeneous and uniform material distribution of the stem no longer being truly isolelastic. In contrast, the implant presented in this work has shown that optimal properties gradients enable the realization of a fully porous implant with properties that mirror the normally changing density of the surrounding proximal femoral bone.

On the other hand, other fully porous materials that commercially available today are less stiff than the solid substrate materials, but do not provide a viable option for creating an isoelastic femoral stem. An example is porous tantalum which is excellent for its biocompatibility, high volumetric porosity, and low modulus of elasticity, but its pore distribution is predominantly

uniform. The reduced stiffness of tantalum foam, in fact, decreases bone resorption; yet, its homogenous distribution of pores has the undesirable effect of increasing interface stresses[44; 54; 55]. In addition, its use in femoral stems can only be as a porous coating on a stiffer solid titanium substrate, precluding a fully porous stem. As a result, most, if not virtually all of the advantages of its low modulus of elasticity, are lost when it is applied for use in a femoral hip stem. The stem design in this study not only addresses the issue of stress shielding by its graded and fully porous design, but also allows the stem to have sufficient strength; its porous architecture is obtained from an aperiodic tessellation of a tetrahedron based unit cell, which has been shown appropriate for load bearing orthopaedic applications [38].

The volumetric index of bone loss has significant clinical relevance since this corresponds to the bone stock available for revision surgeries. We found a reasonably good agreement between the amounts of surface bone loss from FEA and those from DIC experiments. The figures show that FEA results are within statistic values obtained from DIC experiments. We can thus assume the volumetric bone loss measured from simulations can reasonably assess the actual amount of stress shielding that might occur during the DIC experiment. This indicates the reduction of the surface strain is an appropriate proxy for stress shielding.

Although the reduced complexity of the experimental set up shows a promising reduction in stress shielding, cadaveric match pair femurs with physiological loading conditions should be used to reproduce the conditions for which the implant is designed. This is a part of future study. In addition, since the bone loss measured in this study do not account for the adaptive process of bone remodeling over time [56; 57], their values are still representative of the amount of bone resorption from 6 to 24 months postoperatively [58]. Although the majority of bone remodelling occurs within two years, Bone Mass Density can continue to decrease as a result of stress

shielding even up to 14 years after implantation [58]. In this case, the amount of bone resorption can be detected with dual-energy X-ray absorptiometry (DEXA) with a precision of 1-4% [58]. The implications of the work here undertaken are very promising, serving as a multidisciplinary bridge integrating biomechanics, material property tuning, additive manufacturing of 3D porous architecture and clinically relevant experiments, all addressing shortcomings of existing materials for hip prostheses. We have demonstrated that three-dimensional material distributions with variable stiffness can be obtained to develop a hip stem, which is shaped into a minimally invasive geometry. The stem is a short and has a single tapered wedge design, which is the most common implant design type used in North America [59]. In this study, we also showed the effectiveness of using SLM technology to build Ti-6AL-4V controlled gradients of fully porous micro-architected stems.

Unsurprisingly, care must be taken also here with interpreting the results of this work and extrapolate a direct assessment of expected clinical outcomes. Bone resorption is a complex phenomenon involving a multitude of factors specific to the implant, the patient, the surgical procedure, and varying degrees of interaction between the aforementioned factors. It is important to underline that the values reported for stress shielding are percentages of bone that are susceptible to stress shielding immediately post operation, and not necessarily the bone tissue that will resorb in the long term. Although numerical techniques are available to represent this process that is time dependent, at the present time there are no widely-accepted in-vitro biomechanical models available that can represent the phenomenon. As such, further experimental validation of the ability of a tuned fully porous implant to reduce stress shielding should rely upon long term in-vivo models that can account for the biomechanical interaction

complexity of a living system. Future work includes replicating the current investigation in an animal model to examine the long term bone remodelling of a fully porous implant.

## Conclusion

A high strength fully porous material with tunable mechanical properties is introduced for use in minimally invasive hip replacement. The implant microarchitecture is fine-tuned to locally mimic bone tissue properties, which results in minimum bone resorption secondary to stress shielding. This work demonstrates that a high strength fully porous femoral stem with tunable mechanical properties can be designed and manufactured to reduce stress-shielding. The proposed implant has been built successfully with SLM technique while respecting bone ingrowth requirements at the implant interface. The in-vitro test has proved substantial decrease of the femur surface strain, inferring substantial reduction in stress shielding. This development is promising and may possibly pave the way for tuned fully porous materials for bone interfacing implants of next generation use in orthopaedic arthroplasty surgery.

## Acknowledgement

The authors acknowledge the financial support from the Natural Sciences and Engineering Research Council of Canada (NSERC) and the Canadian Institutes of Health Research (CIHR).

# Reference


1. Glassman A, Bobyn J, Tanzer M. 2006. New Femoral Designs Do They Influence Stress Shielding? Clinical Orthopaedics and Related Research 453:64-74.
2. Bobyn J, Mortimer E, Glassman A, et al. 1992. Producing and avoiding stress shielding: laboratory and clinical observations of noncemented total hip arthroplasty. Clinical Orthopaedics and Related Research 274:79-96.
3. Chamay A, Tschantz P. 1972. Mechanical influences in bone remodeling. Experimental research on Wolff's law. Journal of Biomechanics 5:173-180.
4. Sumner DR, Turner TM, Igloria R, et al. 1998. Functional adaptation and ingrowth of bone vary as a function of hip implant stiffness. Journal of Biomechanics 31:909-917.
5. Bugbee WD, CULPEPPER WJ, Engh CA, et al. 1997. Long-Term Clinical Consequences of Stress-Shielding after Total Hip Arthroplasty without Cement*. The Journal of Bone & Joint Surgery 79:1007-1012.
6. Engh Jr CA, Young AM, Engh Sr CA, et al. 2003. Clinical consequences of stress shielding after porous-coated total hip arthroplasty. Clinical orthopaedics and related research 417:157-163.
7. McAuley JP, Culpepper WJ, Engh CA. 1998. Total hip arthroplasty: Concerns with extensively porous coated femoral components. Clinical orthopaedics and related research 355:182-188.
8. Kim Y-H, Kim J-S, Cho S-H. 2001. Strain distribution in the proximal human femur AN IN VITRO COMPARISON IN THE INTACT FEMUR AND AFTER INSERTION OF REFERENCE AND EXPERIMENTAL FEMORAL STEMS. Journal of Bone & Joint Surgery, British Volume 83:295-301.
9. Fernandes PR, Ruben RB, Folgado J. 2010. Bone Implant Design Using Optimization Methods. Biomechanics of Hard Tissues: Wiley-VCH Verlag GmbH & Co. KGaA; pp. 267-296.
10. Ruben R, Folgado J, Fernandes P. 2007. Three-dimensional shape optimization of hip prostheses using a multicriteria formulation. Structural and Multidisciplinary Optimization 34:261-275.
11. Niinimäki T, Junila J, Jalovaara P. 2001. A proximal fixed anatomic femoral stem reduces stress shielding. International orthopaedics 25:85-88.
12. Renkawitz T, Santori FS, Grifka J, et al. 2008. A new short uncemented, proximally fixed anatomic femoral implant with a prominent lateral flare: design rationals and study design of an international clinical trial. BMC musculoskeletal disorders 9:147.
13. Schmidt J, Hackenbroch M. 1994. The Cenos hollow stem in total hip arthroplasty: first experiences in a prospective study. Archives of orthopaedic and trauma surgery 113:117-120.
14. Crowninshield R, Brand R, Johnston R, et al. 1980. An analysis of femoral component stem design in total hip arthroplasty. The Journal of Bone & Joint Surgery 62:68-78.
15. Behrens B, Wirth C, Windhagen H, et al. 2008. Numerical investigations of stress shielding in total hip prostheses. Proceedings of the Institution of Mechanical Engineers, Part H: Journal of Engineering in Medicine 222:593-600.
16. Mattheck C, Vorberg U, Kranz C. 1990. Effects of hollow shaft endoprosthesis on stress distribution in cortical bone. Biomedizinische Technik Biomedical engineering 35:316-319.
17. Hazlehurst KB, Wang CJ, Stanford M. 2013. The potential application of a Cobalt Chrome Molybdenum femoral stem with functionally graded orthotropic structures manufactured using Laser Melting technologies. Medical Hypotheses 81:1096-1099.
18. Hazlehurst KB, Wang CJ, Stanford M. 2014. A numerical investigation into the influence of the properties of cobalt chrome cellular structures on the load transfer to the periprosthetic femur following total hip arthroplasty. Medical engineering & physics 36:458-466.

19. Murr L, Gaytan S, Medina F, et al. 2010. Next-generation biomedical implants using additive manufacturing of complex, cellular and functional mesh arrays. Philosophical Transactions of the Royal Society A: Mathematical, Physical and Engineering Sciences 368:1999-2032.
20. Marcellin-Little DJ, Cansizoglu O, Harrysson OL, et al. 2010. In vitro evaluation of a low-modulus mesh canine prosthetic hip stem. American journal of veterinary research 71:1089-1095.
21. Arabnejad S, Pasini D. 2012. Multiscale Design and Multiobjective Optimization of Orthopedic Hip Implants with Functionally Graded Cellular Material. Journal of Biomechanical Engineering 134:031004.
22. Arabnejad S, Pasini D. 2013. The Fatigue Design of a Bone Preserving Hip Implant With Functionally Graded Cellular Material. Journal of Medical Devices 7:020907.
23. Harrison N, McHugh P, Curtin W, et al. 2013. Micromotion and friction evaluation of a novel surface architecture for improved primary fixation of cementless orthopaedic implants. Journal of the Mechanical Behavior of Biomedical Materials 21:37-46.
24. Marin E, Fusi S, Pressacco M, et al. 2010. Characterization of cellular solids in Ti6Al4V for orthopaedic implant applications: Trabecular titanium. Journal of the mechanical behavior of biomedical materials 3:373-381.
25. Khanoki SA, Pasini D. 2012. Multiscale Design and Multiobjective Optimization of Orthopedic Hip Implants with Functionally Graded Cellular Material. Journal of Biomechanical Engineering 134:031004.
26. Arabnejad Khanoki S, Pasini D. 2013. Fatigue design of a mechanically biocompatible lattice for a proof-of-concept femoral stem. Journal of the Mechanical Behavior of Biomedical Materials 22:65-83.
27. Cheng XY, Li SJ, Murr LE, et al. 2012. Compression deformation behavior of Ti–6Al–4V alloy with cellular structures fabricated by electron beam melting. Journal of the Mechanical Behavior of Biomedical Materials 16:153-162.
28. Parthasarathy J, Starly B, Raman S, et al. 2010. Mechanical evaluation of porous titanium (Ti6Al4V) structures with electron beam melting (EBM). Journal of the Mechanical Behavior of Biomedical Materials 3:249-259.
29. Xia Z, Zhou C, Yong Q, et al. 2006. On selection of repeated unit cell model and application of unified periodic boundary conditions in micro-mechanical analysis of composites. International Journal of Solids and Structures 43:266-278.
30. Mullen L, Stamp R, Fox P, et al. 2009. Selective laser melting: A unit cell approach for the manufacture of porous, titanium, bone in-growth constructs, suitable for orthopedic applications. II. Randomized structures. Journal of Biomedical Materials Research Part B: Applied Biomaterials 92:178-188.
31. Ahmadi S, Campoli G, Amin Yavari S, et al. 2014. Mechanical behavior of regular open-cell porous biomaterials made of diamond lattice unit cells. Journal of the Mechanical Behavior of Biomedical Materials 34:106-115.
32. Eldesouky I, Abdelaal O, El-Hofy H. 2014. Femoral hip stem with additively manufactured cellular structures. Biomedical Engineering and Sciences (IECBES), 2014 IEEE Conference on: IEEE; pp. 181-186.
33. Speirs AD, Heller MO, Duda GN, et al. 2007. Physiologically based boundary conditions in finite element modelling. Journal of Biomechanics 40:2318-2323.
34. Heller MO, Bergmann G, Kassi JP, et al. 2005. Determination of muscle loading at the hip joint for use in pre-clinical testing. Journal of Biomechanics 38:1155-1163.
35. Austman RL, Milner JS, Holdsworth DW, et al. 2008. The effect of the density–modulus relationship selected to apply material properties in a finite element model of long bone. Journal of biomechanics 41:3171-3176.

36. Baca V, Horak Z, Mikulenka P, et al. 2008. Comparison of an inhomogeneous orthotropic and isotropic material models used for FE analyses. Medical engineering & physics 30:924-930.
37. Peng L, Bai J, Zeng X, et al. 2006. Comparison of isotropic and orthotropic material property assignments on femoral finite element models under two loading conditions. Medical engineering & physics 28:227-233.
38. Arabnejad S, Burnett Johnston R, Pura JA, et al. High-strength porous biomaterials for bone replacement: A strategy to assess the interplay between cell morphology, mechanical properties, bone ingrowth and manufacturing constraints. Acta Biomaterialia.
39. Masoumi Khalil Abad E, Arabnejad Khanoki S, Pasini D. 2013. Fatigue design of lattice materials via computational mechanics: Application to lattices with smooth transitions in cell geometry. International Journal of Fatigue 47:126-136.
40. Arabnejad S, Pasini D. 2013. Mechanical properties of lattice materials via asymptotic homogenization and comparison with alternative homogenization methods. International Journal of Mechanical Sciences 77:249-262.
41. Arabnejad S, Pasini D. 2013. Mechanical properties of lattice materials via asymptotic homogenization and comparison with alternative homogenization methods. International Journal of Mechanical Sciences 77:249-262.
42. Nicholas T, Zuiker J. 1989. On the use of the Goodman diagram for high cycle fatigue design. International Journal of Fracture 80:219-235.
43. Weinans H, Huiskes R, Grootenboer H. 1992. Effects of material properties of femoral hip components on bone remodeling. Journal of Orthopaedic Research 10:845-853.
44. Kuiper J, Huiskes R. 1992. Numerical optimization of hip-prosthetic stem material. Recent Advances in Computer Methods in Biomechanics & Biomedical Engineering J Mddleton, GN Pande, and KR Williams:76–84.
45. Heiner AD. 2008. Structural properties of fourth-generation composite femurs and tibias. Journal of Biomechanics 41:3282-3284.
46. Gruen TA, Mcneice GM, Amstutz HC. 1979. " Modes of failure" of cemented stem-type femoral components: a radiographic analysis of loosening. Clinical Orthopaedics and Related Research 141:17-27.
47. Banaszkiewicz PA. 2014. Clinical and Radiographic Evaluation of Total Hip Replacement. A Standard System of Terminology for Reporting Results. Classic Papers in Orthopaedics: Springer; pp. 23-26.
48. Johnston RC, Fitzgerald R, Harris W, et al. 1990. Clinical and radiographic evaluation of total hip replacement. A standard system of terminology for reporting results. J Bone Joint Surg Am 72:161-168.
49. Bombelli R, Mathys R. 1982. Cementless isoelastic RM total hip prosthesis. Journal of the Royal Society of Medicine 75:588.
50. Trebse R, Milosev I, Kovac S, et al. 2005. Poor results from the isoelastic total hip replacement. Acta Orthopaedica 76:169-176.
51. Glassman AH, Crowninshield RD, Schenck R, et al. 2001. A low stiffness composite biologically fixed prosthesis. Clinical orthopaedics and related research 393:128.
52. Hartzband M, Glassman A, Goldberg V, et al. 2010. Survivorship of a Low-stiffness Extensively Porous-coated Femoral Stem at 10 Years. Clinical Orthopaedics and Related Research® 468:433-440.
53. Akhavan S, Matthiesen MM, Schulte L, et al. 2006. Clinical and histologic results related to a low-modulus composite total hip replacement stem. The Journal of Bone and Joint Surgery (American) 88:1308-1314.
54. Khanoki SA, Pasini D. 2011. Multiscale Design and Multiobjective Optimization of Orthopaedic Cellular Hip Implants. Proceedings of the ASME 2011 International Design

Engineering Technical Conferences & Computers and Information in Engineering Conference IDETC/CIE 2011. Washington, DC, USA.
55. Kuiper J, Huiskes R. 1996. Friction and stem stiffness affect dynamic interface motion in total hip replacement. Journal of Orthopaedic Research 14:36-43.
56. Huiskes R, Weinans H, Grootenboer HJ, et al. 1987. Adaptive bone-remodeling theory applied to prosthetic-design analysis. Journal of Biomechanics 20:1135-1150.
57. Bouguecha A, Elgaly I, Stukenborg-Colsman C, et al. 2010. Numerical Investigations of the Strain-Adaptive Bone Remodeling in the Prosthetic Pelvis. Springer; pp. 562-565.
58. Bodén HS, Sköldenberg OG, Salemyr MOf, et al. 2006. Continuous bone loss around a tapered uncemented femoral stem: a long-term evaluation with DEXA. Acta Orthopaedica 77:877-885.
59. Berry DJ, Bozic KJ. 2010. Current practice patterns in primary hip and knee arthroplasty among members of the American Association of Hip and Knee Surgeons. The Journal of arthroplasty 25:2-4.

# Figure captions

**Figure 1**: A) Physiological FEA of the implanted femur. B) Computational scheme for multiscale mechanics and material property optimization of a minimally invasive 3D hip implant with minimum bone resorption. C) Optimum relative density distribution of the fully porous implant. D) Generation of lattice microarchitecture from optimal relative density distribution using a high strength tetrahedron topology. E) Implant manufacturing via Selective Laser Melting.

**Figure 2:** A) Implant manufacturing via Selective Laser Melting. B) Micro CT assessment of the implant lattice.

**Figure 3:** A) In-vitro assessment of stress shielding using Digital Image Correlation (DIC) and B) FE model of DIC test.

**Figure 4**: Regions prone to bone resorption in Gruen zones 1 to 7 for (A) fully solid implant and for (B) fully porous implant with tailored relative density distribution. Values presented here are volume bone loss measured based on metrics presented in the Supporting Information S5. All zones with no reported bone resorption are 0%.

**Figure 5:** (A) Surface bone loss measurement obtained from DIC experiment. (B) Surface and volume bone loss measurement from the FE model reproducing the condition of the experiment set-up. Surface bone loss is considered when the ratio of post implantation surface strain squared to the pre implantation surface strain squared decreases more than 75%. Volume bone loss is measured when the ratio of post implantation strain energy to the pre implantation strain energy decreases more than 75%.

# Table captions

**Table 1**: Forces, acting forces points, and boundary conditions applied to the intact and implanted femur during the gait cycle (taken from [33; 34]).